CIAO1 loss of function causes a neuromuscular disorder with compromise of nucleocytoplasmic Fe-S enzymes

Nunziata Maio[1†], Rotem Orbach[2†], Irina T. Zaharieva[3†], Ana Töpf[4], Sandra Donkervoort[2], Pinki Munot[3], Juliane Mueller[3], Tracey Willis[5,6], Sumit Verma[7], Stojan Peric[8], Deepa Krishnakumar[9], Sniya Sudhakar[10], A. Reghan Foley[2], Sarah Silverstein[2], Ganka Douglas[11], Lynn Pais[12], Stephanie DiTroia[12], Christopher Grunseich[2], Ying Hu[2], Caroline Sewry[3, 5], Anna Sarkozy[3], Volker Straub[4], Francesco Muntoni[3], Tracey A. Rouault[1,✉], Carsten G. Bönnemann[2,✉]

[†]These authors contributed equally to this work.

Author affiliations:

1 Molecular Medicine Branch, *Eunice Kennedy Shriver* National Institute of Child Health and Human Development, Bethesda, Maryland 20892, USA.

2 National Institutes of Health, Neuromuscular and Neurogenetic Disorders of Childhood Section, Bethesda, Maryland 20892, USA.

3 Dubowitz Neuromuscular Centre, UCL Great Ormond Street Institute of Child Health, London, WC1N 1EH, UK.

4 John Walton Muscular Dystrophy Research Centre, Translational and Clinical Research Institute, Newcastle University and Newcastle Hospitals NHS Foundation Trust, Newcastle upon Tyne, UK.

5 Wolfson Centre for Neuromuscular Disorders, Robert Jones and Agnes Hunt Orthopaedic Hospital, Oswestry, SY10 7AG, UK.

6 Chester University, The Robert Jones and Agnes Hunt Orthopaedic Hospital, NHS Foundation Trust, Oswestry, Shropshire, SY10 7AG, UK.

7 Department of Pediatrics and Neurology, Emory University School of Medicine, Georgia, Atlanta, USA.

8 Department for Neuromuscular Disorders, Neurology Clinic, University Clinical Centre of Serbia, Faculty of Medicine, University of Belgrade, Belgrade, Serbia.

9 Paediatric Neurology, Addenbrooke's Hospital, Cambridge University Hospitals NHS Foundation Trust, Cambridge, UK.

10 Department of Neuroradiology, Great Ormond Street NHS Trust Hospital, London

11 GeneDx, LLC, Gaithersburg, MD 20877, USA.

12 Program in Medical and Population Genetics, Center for Mendelian Genomics, Broad Institute of MIT and Harvard, Cambridge, MA, USA.

✉ Correspondence to: Carsten Bönnemann, MD E-mail: carsten.bonnemann@nih.gov

Full address: Neuromuscular and Neurogenetic Disorders of Childhood Section Neurogenetics Branch, National Institute of Neurological Disorders and Stroke NIH, Building 10, Room 2B39, 10 Center Drive, Bethesda, MD 20892-1477, USA.

✉ Correspondence to: Tracey Ann Rouault, MD E-mail: rouault@mail.nih.gov

Full address: Molecular Medicine Branch, *Eunice Kennedy Shriver* National Institute of Child Health and Human Development, NIH, Building 35A, Room 2D824, 9000 Rockville Pike, Bethesda, MD, 20892, USA.

Inventory of Supplemental Information

Supplemental figures

Supplemental Tables

Supplemental references

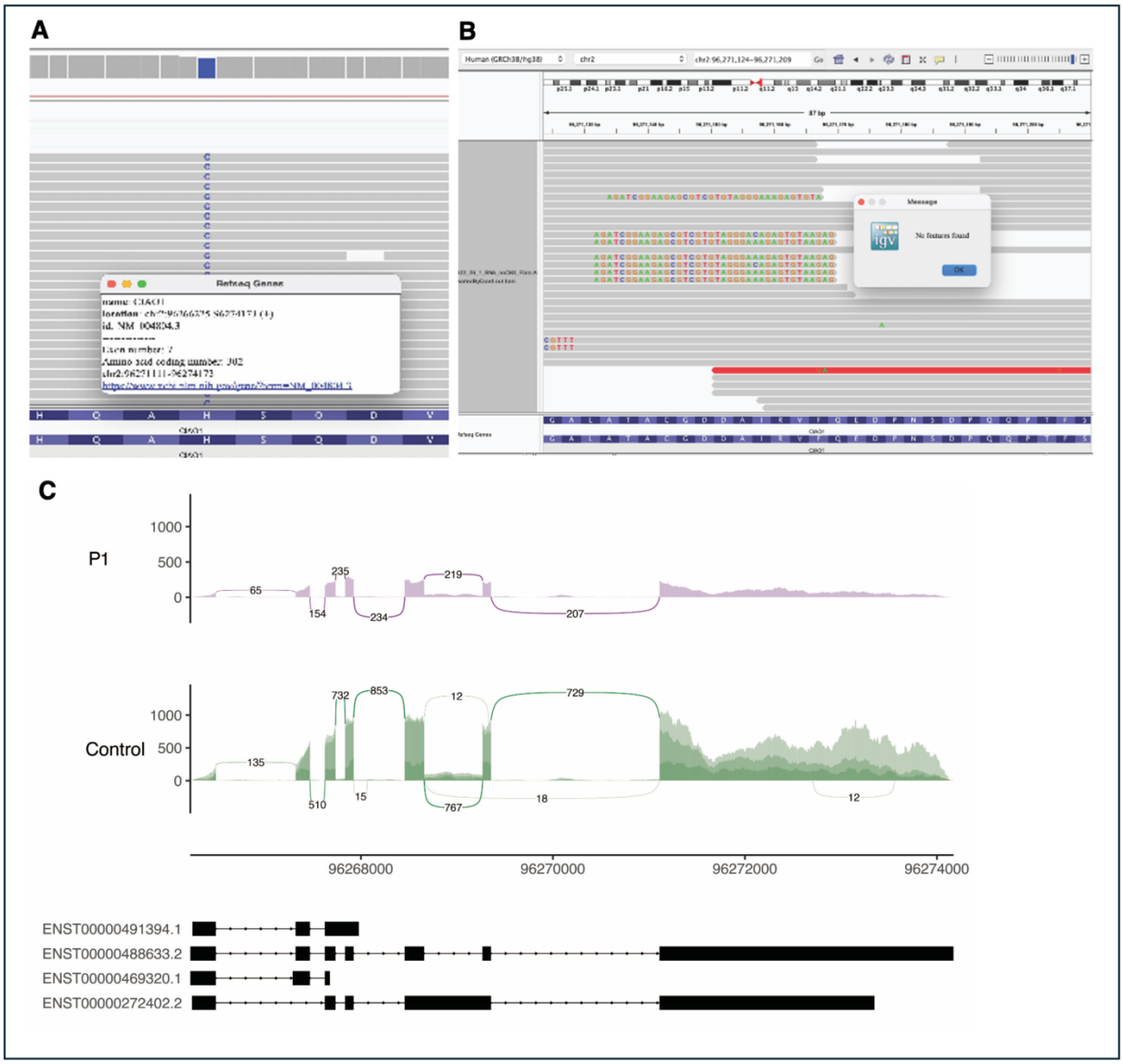

Supplemental Figure 1. RNA sequencing of P1 fibroblasts. A. Maternal allele appears to be homozygous in P1 RNA-seq sample. **B.** Soft clipping in exon 7 do not map, showing that there is no evidence for paternal reads due to nonsense mediated decay of the truncated mRNA. **C.** Sashimi plots comparing *CIAO1* sequencing reads in P1 (purple) and three control fibroblasts samples (green).

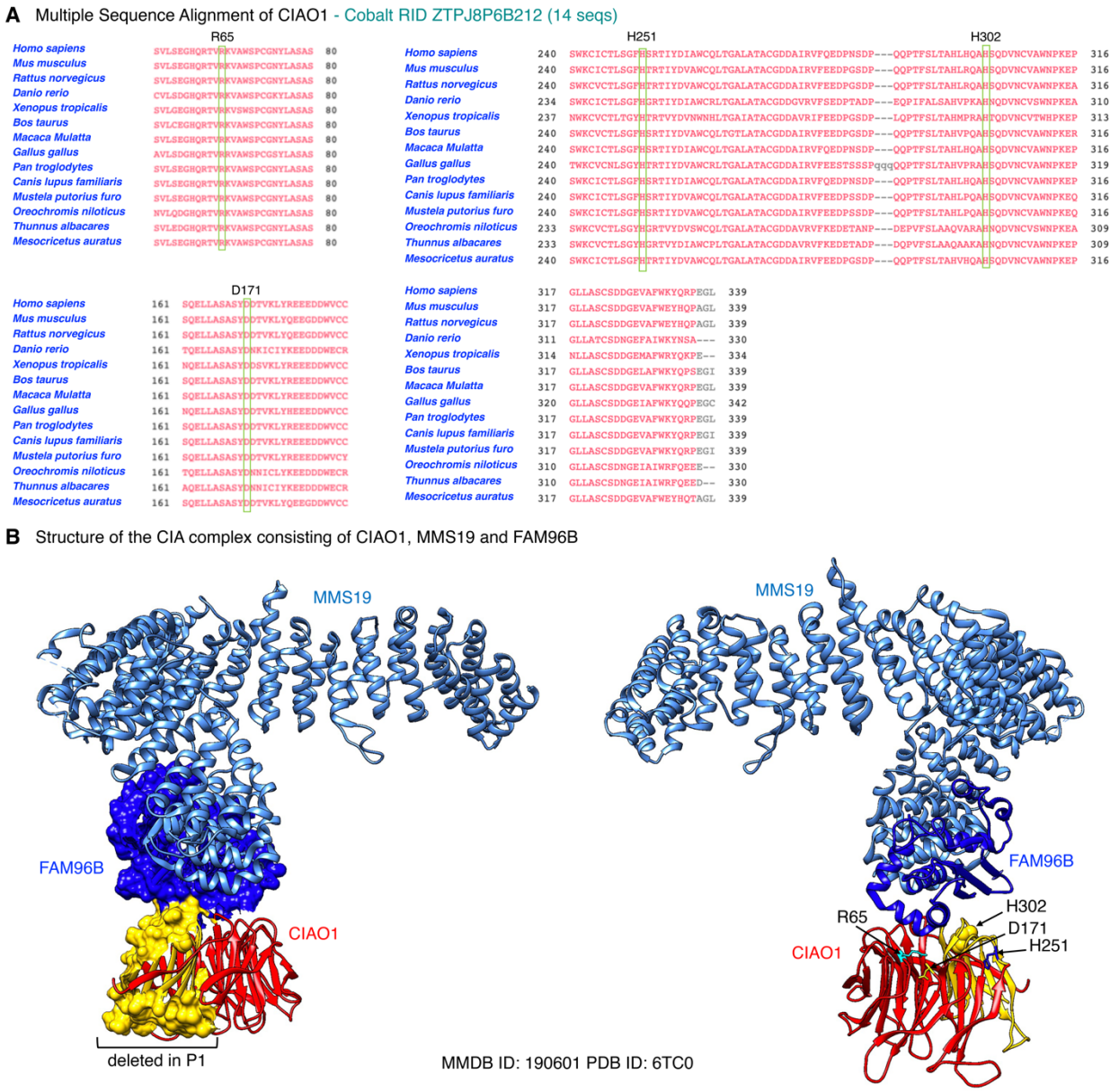

Supplemental Figure 2. Multiple sequence alignment of CIAO1 amino acid sequences and location of the amino acid residues altered in patients. A. Multiple sequence alignment of CIAO1 sequences generated with Constraint-based Multiple Alignment Tool (COBALT, NCBI), showing complete conservation across different species of the amino acid residues altered in the patients. **B.** 3D structure of the CIA complex consisting of CIAO1, MMS19 and FAM96B (PDB ID: 6TC0). On the left, CIAO1 is shown in ribbon- and surface- mode representations and colored in red, except for the domain deleted in P1 which is rendered in surface-mode representation and colored in yellow. On the right, CIAO1 is shown in ribbon-mode representation and the location of amino acid residues altered in the patients are labeled and pointed by arrows.

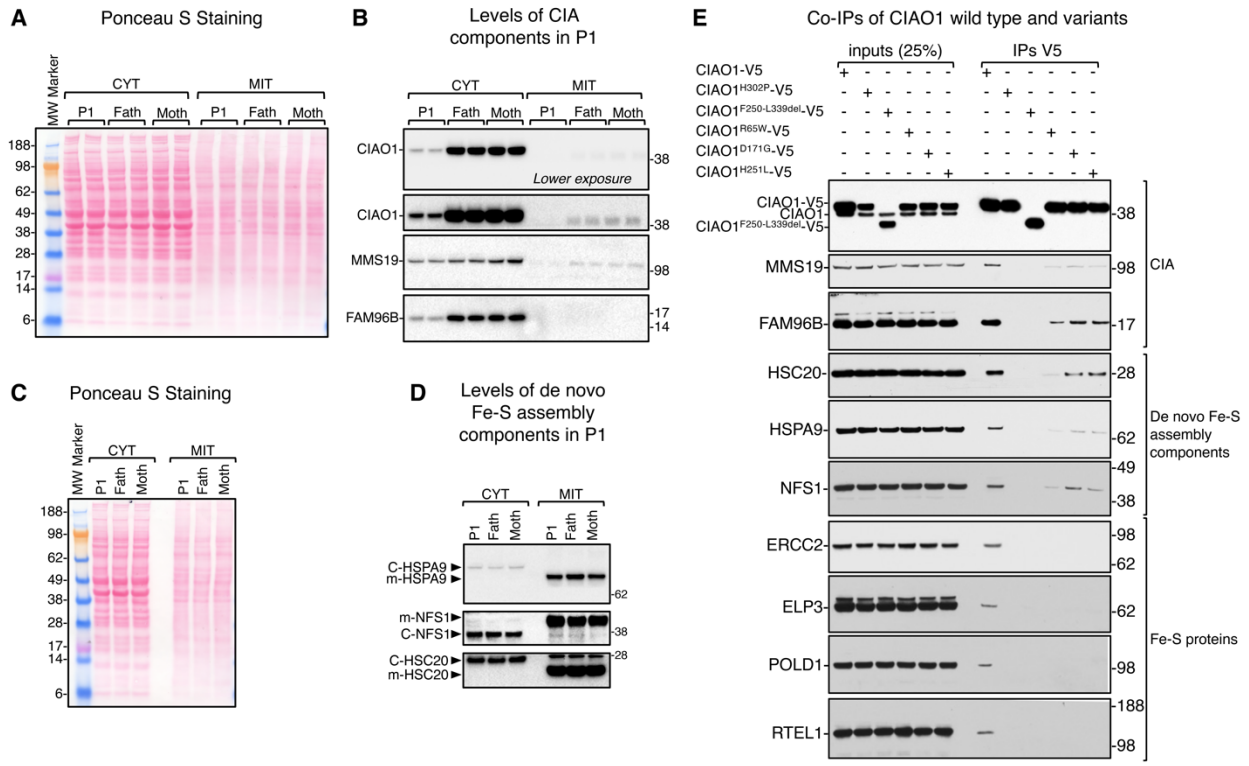

Supplemental Figure 3. The CIAO1 variants identified in patients have greatly diminished stability compared to wild type CIAO1 and impaired binding to the components of the Fe-S biogenesis machinery and recipient apo-proteins. A. Ponceau S staining of nitrocellulose membrane allows visualization of proteins extracted from cytosolic (CYT) and mitochondrial (MIT) lysates obtained from P1- and parental- derived fibroblasts. MW marker (molecular weight marker). **B.** Immunoblots to components of the CIA machinery shows specific cytosolic (but not mitochondrial) localization of CIAO1, MMS19 and FAM96B. Levels of these components were profoundly diminished in P1 cytosolic lysates compared to parental derived fibroblasts. **C.** Ponceau S staining of nitrocellulose membrane allows visualization of proteins extracted from cytosolic (CYT) and mitochondrial (MIT) lysates obtained from P1- and parental-derived fibroblasts. **D.** Immunoblots to components of the *de novo* Fe-S cluster biogenesis machinery shows dual localization to cytosol (CYT) and mitochondria (MIT) of HSPA9, HSC20 and NFS1, consistent with previously reported results.(1-3) **E.** Co-immunoprecipitation (co-IP) experiments of recombinantly expressed V5-tagged *CIAO1* wild type and variants identified in patients, as indicated. In order to normalize for the reduced stability of the CIAO1-V5 variants, the V5 agarose beads incubated with the lysates obtained from cells expressing the variants were recovered in 25µl of elution buffer (EB), whereas 65µl of EB were used for the wild-type sample. (A-E, *n*= 3 biological replicates).

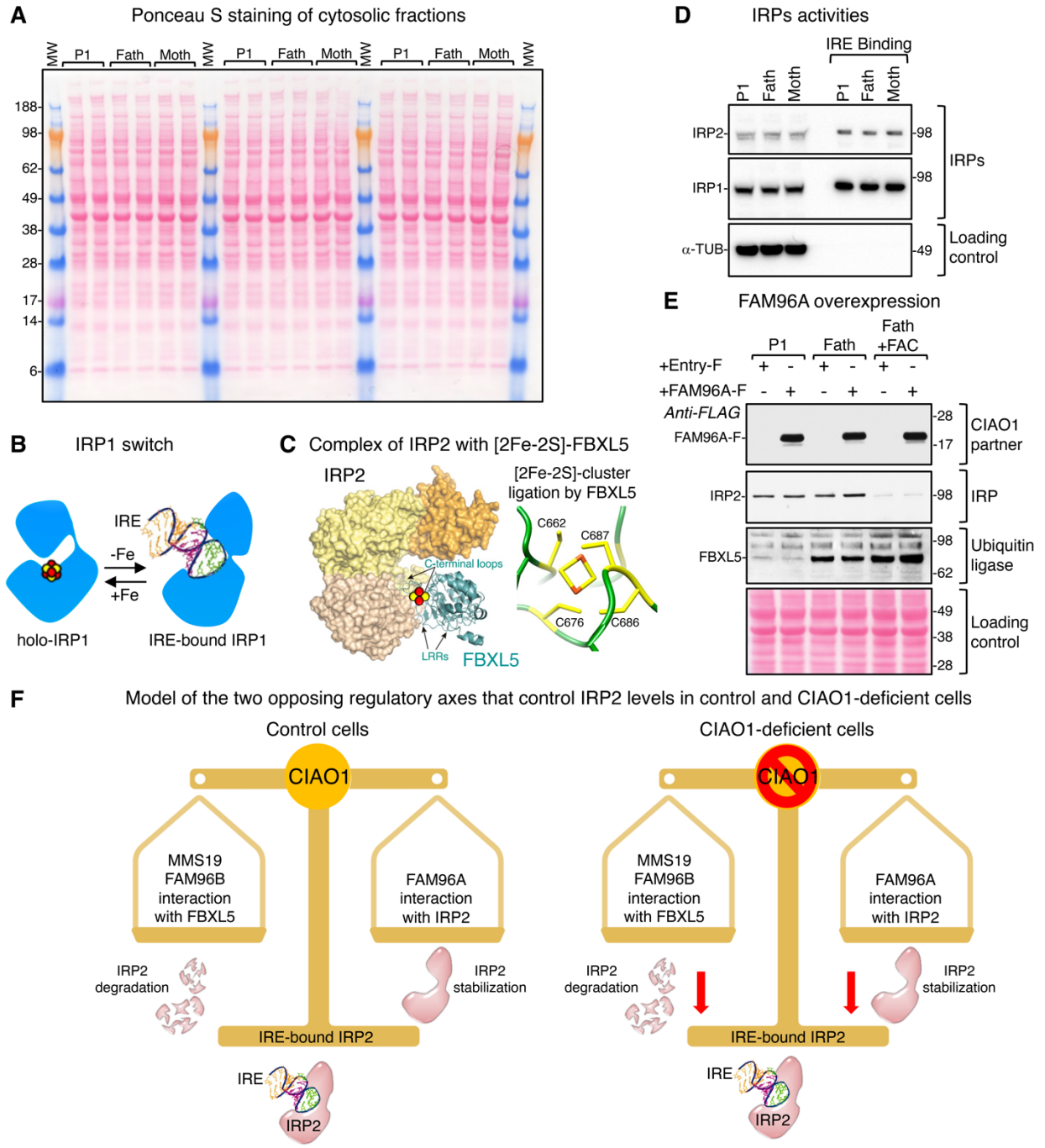

Supplemental Figure 4. Iron homeostasis is maintained in patient-derived cells because of two opposing regulatory axes that are at equilibrium. A. Ponceau S staining of nitrocellulose membrane allows visualization of proteins extracted from cytosolic lysates obtained from P1- and parental- derived fibroblasts (*n*=4 biological replicates). The membrane was probed with antibodies as shown in Figure 4, panels A, B and G. MW designates the molecular weight marker. **B.** IRP1, a protein with dual function. IRP1 alternates between a cytosolic aconitase holo-form when it ligates a [4Fe-4S] cluster in its active site cleft under iron replete conditions (+Fe) and an apo-protein that lacks the cluster and binds to Iron Responsive Element (IRE) stem-loop structures

present in several transcripts encoding iron metabolism proteins under iron deficiency (-Fe). Upon binding, IRP1 represses translation of transcripts that contain IREs near the 5'-end (e.g., ferritin H and L) and stabilizes from endonucleolytic degradation mRNAs that contain IREs at the 3'-UTR (e.g., transferrin receptor). **C.** Complex of IRP2 with its ubiquitin-ligase FBXL5. FBXL5 has been reported to interact with the CIA complex(4) and to ligate a [2Fe-2S] cluster.(5) **D.** IRE-binding activities of IRP1 and IRP2 in P1- and parental-derived fibroblasts (*n*=3 biological replicates). **E.** Overexpression of C-terminally FLAG-tagged FAM96A (+FAM96A-F) in P1 and parental-derived cells. Treatment of control cells (P1's father-derived fibroblasts) with 100 μM ferric ammonium citrate (FAC), as an iron source, was included to elicit IRP2 degradation. Transfection with the empty vector (+Entry-F) was included as a control. Overexpression of FAM96A, in the absence of CIAO1, in P1-derived cells failed to stabilize IRP2 (*n*=3 biological replicates). **F.** Model depicting the two opposing regulatory axes which control maintenance of IRP2 protein levels and iron homeostasis in the CIAO1-deficient patient-derived cells. Two multi-protein complexes that share CIAO1 as a component control IRP2 protein levels and cellular iron homeostasis. In control cells (on the left), levels of IRP2 result from a balance of two opposing regulatory axes: degradation of IRP2 by FBXL5 and stabilization of IRP2 through its interaction with the CIAO1/FAM96A complex. Under steady state conditions:

1. IRP2 is degraded by FBXL5 whose levels and ubiquitin-ligase activity depend on its ability to interact with CIAO1, FAM96B and MMS19(4) (left arm of the balance);

2. IRP2 is stabilized by its interaction with the CIAO1/FAM96A complex(6) (right arm of the balance).

In the patient-derived cells (on the right), loss of CIAO1 prevents the regular turnover of IRP2 (left arm of the balance) because of the decreased levels of FBXL5. Loss of FBXL5 would be expected to cause an increase in IRP2 protein levels. However, because of the compromised stabilization of IRP2 due to loss of CIAO1 and FAM96A, levels of IRP2 remain unchanged in the patient-derived cells compared to control. The rate of IRP2 degradation is decreased in the patient-derived cells, while its stabilization is concomitantly impaired, resulting in no significant change in IRP2 levels under steady state conditions.

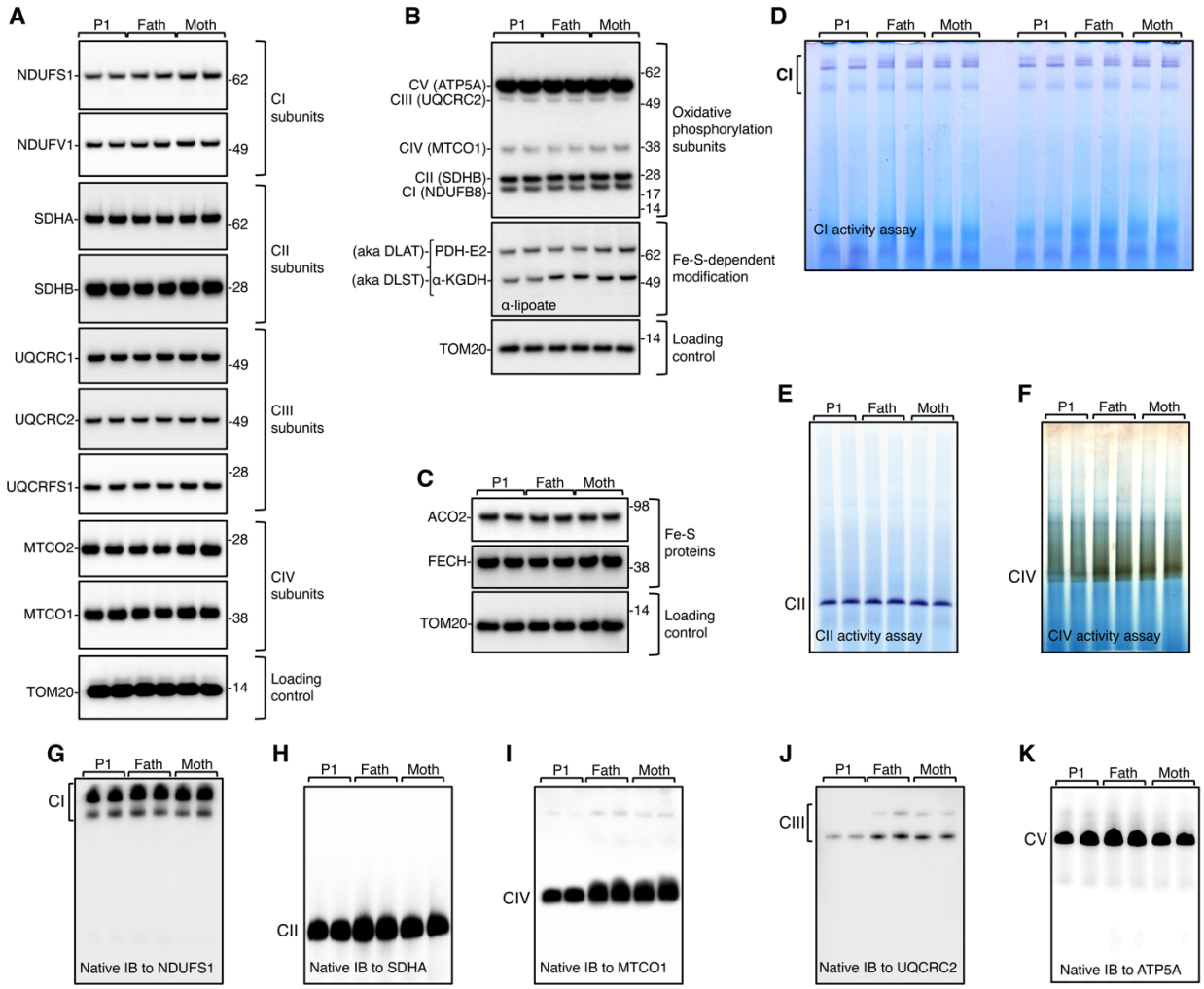

Supplemental Figure 5. P1-derived fibroblasts do not exhibit a profound mitochondrial defect. A. SDS immunoblots to subunits of mitochondrial respiratory complex I (NDUFS1, NDUFV1), complex II (SDHA, SDHB), complex III (UQCRC1, UQCRC2, UQCRFS1), and complex IV (MTCO1, MTCO2) in lysates obtained from P1- and parental- derived fibroblasts. Levels of TOM20 are shown as a reference for loading control. **B.** SDS immunoblots to total oxidative phosphorylation subunits, as indicated, and to lipoate in P1- and parental- derived cells. **C.** SDS immunoblots to the mitochondrial Fe-S cluster subunits aconitase (ACO2) and to the terminal heme biosynthetic enzyme ferrochelatase (FECH) in P1- and parental- derived fibroblasts. **D.** In-gel NADH oxidase (diaphorase) activity assay of mitochondrial complex I (CI) in P1- and parental-derived cells. **E.** In-gel succinate dehydrogenase (CII) activity assay in P1- and parental- derived cells. **F.** In-gel cytochrome c oxidase (CIV) activity assay in P1- and parental-derived fibroblasts. **G-K.** Native immunoblots to NDUFS1 (complex I subunit), SDHA (complex II subunit), MTCO1 (complex IV subunit), UQCRC2 (complex III subunit) and ATP5A (complex V subunit), respectively, in P1- and parental-derived fibroblasts to assess the overall levels of fully assembled respiratory complexes. (A-K, *n*=3 biological replicates).

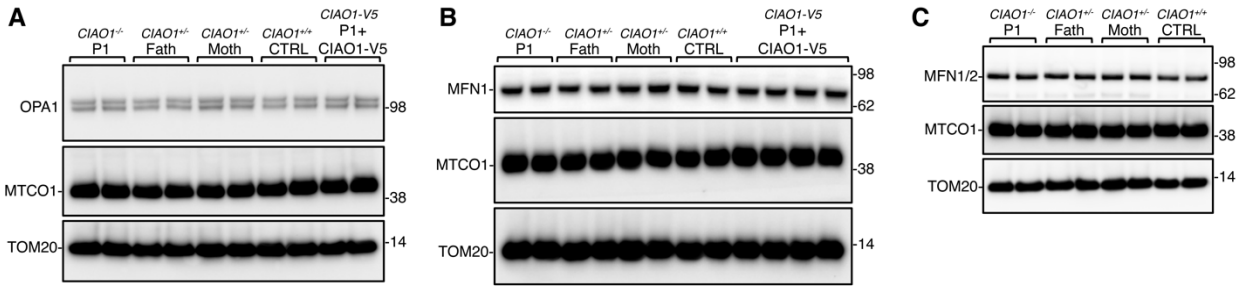

Supplemental Figure 6. Levels of the regulators of mitochondrial dynamics, OPA1 and mitofusin 1 and 2 (MFN1/2), were unaltered in P1- derived fibroblasts. A. Immunoblots to OPA1 and the complex IV subunit MTCO1 in P1-, parental-, control- (corresponding to fibroblasts expressing two wild type copies of *CIAO1*) fibroblasts and in P1- derived fibroblasts that had been lentivirally transduced with V5-tagged *CIAO1* wild type. **B.** Immunoblots to MFN1 and the complex IV subunit MTCO1 in P1-, parental-, control- (corresponding to fibroblasts expressing two wild type copies of *CIAO1*) fibroblasts and in P1- derived fibroblasts that had been lentivirally transduced with V5-tagged *CIAO1* wild type. **C.** Immunoblots to MFN1, MFN2 and the complex IV subunit MTCO1 in P1-, parental-, control- (corresponding to fibroblasts expressing two wild type copies of *CIAO1*) fibroblasts and in P1- derived fibroblasts that had been lentivirally transduced with V5-tagged *CIAO1* wild type. In **A-C**, levels of TOM20 are presented as a reference for loading control. (A-C, *n*=3 biological replicates).

Table S1. Predicted pathogenicity of *CIAO1* variants identified in patients

Chromosomal location[1]	*CIAO1* Variant[2]	Patient identifiers (number of alleles)	gnomAD[3]	gnomAD – number of homozygous[3]	ExAC2[4]	REVEL[5]	Polyphen2[6]	SIFT[7]
chr2: 96936974	c.905A>C p.His302Pro	P1, P2, P3 (n = 3)	0.00002121	0	0.000008246	Deleterious (Strong) (0.95)	Deleterious (Moderate) (1)	Uncertain (0.003)
chr2: 96933112	c.193C>T p.Arg65Trp	P2, P3 (n = 2)	0.001011	0	0.0009243	Uncertain (0.45)	Deleterious (Moderate) (1)	Deleterious (Supporting) (0)
chr2: 96934217	c.512A>G p.Asp171Gly	P4 (n = 1)	0	n/a	0	Deleterious (Moderate) (0.93)	n/a	Deleterious (Supporting) (0)
chr2: 96935066	c.752A>T p.His251Leu	P4 (n = 1)	0.000003976	0	0.000008237	Deleterious (Moderate) (0.92)	Deleterious (Supporting) (1)	Uncertain (0.002)
chr2:96936630-96937369	DEL: chr2:96936630-96937369 p.Phe250_Leu339del	P1 (n=1)	0	n/a	0	n/a	n/a	n/a

[1]reference sequence: NM_004804.3
[2]hg19
[3]gnomAD v2.1.1: 141,456 samples
[4]ExAC v1.0: 60,706 samples
[5]REVEL, Ensemble Method for Predicting the Pathogenicity of Rare Missense Variant based on a combination of scores from 13 individual tools; https://sites.google.com/site/revelgenomics/
[6]Polyphen2, predicts possible impact of an amino acid substitution on the structure and function of a human protein; http://genetics.bwh.harvard.edu/pph2/
[7]SIFT, predicts whether an amino acid substitution affects protein function based on sequence homology and the physical properties of amino acids; https://sift.bii.a-star.edu.sg/

Supplemental references

1. Maio N, Singh A, Uhrigshardt H, Saxena N, Tong WH, and Rouault TA. Cochaperone binding to LYR motifs confers specificity of iron sulfur cluster delivery. *Cell Metab.* 2014;19(3):445-57.
2. Kim KS, Maio N, Singh A, and Rouault TA. Cytosolic HSC20 integrates de novo iron-sulfur cluster biogenesis with the CIAO1-mediated transfer to recipients. *Hum Mol Genet.* 2018;27(5):837-52.
3. Maio N, and Rouault TA. Outlining the Complex Pathway of Mammalian Fe-S Cluster Biogenesis. *Trends Biochem Sci.* 2020;45(5):411-26.
4. Mayank AK, Pandey V, Vashisht AA, Barshop WD, Rayatpisheh S, Sharma T, et al. An Oxygen-Dependent Interaction between FBXL5 and the CIA-Targeting Complex Regulates Iron Homeostasis. *Mol Cell.* 2019;75(2):382-93 e5.
5. Wang H, Shi H, Rajan M, Canarie ER, Hong S, Simoneschi D, et al. FBXL5 Regulates IRP2 Stability in Iron Homeostasis via an Oxygen-Responsive [2Fe2S] Cluster. *Mol Cell.* 2020;78(1):31-41 e5.
6. Johnson NB, Deck KM, Nizzi CP, and Eisenstein RS. A synergistic role of IRP1 and FBXL5 proteins in coordinating iron metabolism during cell proliferation. *J Biol Chem.* 2017;292(38):15976-89.